Silicon Based Waveguides

Robert J. Bozeat, S. Day, F. Hopper, F. P. Payne,
S. W. Roberts, and M. Asghari

Bookham Technology plc, Oxfordshire, UK

Abstract. Optical waveguide based devices are key to the operation of many modern optical communication systems. The following chapter outlines the design and application of optical waveguides of the Silicon On Insulator (SOI) type. The important properties of these waveguides are described, the design choices that must be made and their implications are highlighted. The interfacing of silicon waveguides to single mode optical fibres by the use of mode transforming tapers is described and the design methodology behind the production of adiabatic tapers is discussed. Finally the design of Arrayed Waveguide Gratings (AWGs) and Variable Optical Attenuators (VOAs) in silicon waveguide technology is outlined.

1 Introduction

Devices incorporating planar optical waveguides are increasingly finding application within modern data communication and telecommunication systems. These devices may be found multiplexing and demultiplexing signals within Dense Wavelength Division Multiplexed (DWDM) systems [1], switching and routing within reconfigurable system nodes [2] or gain equalising within fibre amplifiers [3].

Much of the early research work into planar waveguide technology was focussed around the lithium niobate material system. Research interest was driven by lithium niobate's large linear electro-optic effect (Pockels effect) and hence potential for the production of electro-optic waveguide modulators [4]. Lithium niobate has subsequently developed into a commercially mature high speed modulator technology. In the 1980s research interest began to focus upon Silica-on-Silicon [5] and Silicon-on-Insulator (SOI) [6] as material systems that were perceived to offer greater potential for the fabrication of more complex waveguide based devices.

Silica-on-Silicon waveguides confine the propagating radiation within multilayer doped silica films that are deposited onto standard, microelectronics grade, silicon substrates. The composition of the waveguiding materials and the geometry of the waveguiding structure are normally chosen to enable the straightforward, low loss interfacing to standard single mode optical fibre. Low index contrast waveguides of this type do not however yield compact devices due to the large bend radii that must be employed. Higher index contrast glasses offer the potential for more compact devices [7] but interfacing these waveguides to single mode fibres is problematic.

L. Pavesi, D. J. Lockwood (Eds.): Silicon Photonics, Topics Appl. Phys. **94**, 269–295 (2004)

SOI waveguides confine the propagating radiation within an epitaxially grown, single crystal, silicon film which has an implanted lower oxide cladding. These high index contrast waveguides offer the potential for small radius waveguide bends and hence highly compact components. In addition active devices are possible because silicon can be made optically absorbent at infrared wavelengths [8] either by doping or by carrier injection. The efficient coupling of SOI waveguides to standard single mode optical fibres is possible but requires careful interface design.

The following will focus specifically upon optical waveguides fabricated in SOI materials. After a brief introduction to the material system a selective account of historical developments in the field will be given. The design of passive waveguides for the realisation of compact bends and low birefringence will be described. Finally the interfacing of SOI waveguides to single mode fibre will then be considered and some example devices will be described.

2 Background

Silicon on insulator materials have been an active area of research since the early 1960s. Research interest was initially stimulated by the potential of these materials for the production of high speed and radiation hard CMOS microelectronic circuits [9]. Early SOI substrates were largely of the Silicon-on-Sapphire (SOS) type comprising of a thin layer of silicon which was deposited onto the surface of a sapphire substrate wafer. Unfortunately SOS substrates tended to suffer from poor quality silicon layers due to the lattice mismatch between silicon and sapphire. In the late 1970s the SIMOX technique was first used for the production of SOI wafers. SIMOX wafers have a buried silicon dioxide insulating layer that is formed using a multiple oxygen implantation and annealing process. It was found to be possible to achieve high quality silicon surface layers using the SIMOX approach. More recently direct wafer bonding [10] has emerged as an attractive alternative to the SIMOX process for the production of SOI wafers with thick silicon surface layers. SOI wafers of both bonded and SIMOX types are now widely available, commercial products.

Research interest in SIMOX as a waveguiding material dates from the late 1980s. SIMOX waveguides were first fabricated from wafers with sub-micron silicon surface layers [11]. The dimensions of these waveguides were consistent with the dimensions required for single moded operation in SOI slab waveguides. In 1991 *Soref* et al. [12] described single moded SOI waveguides with much larger cross sectional dimensions where shallow etched ribs were used to provide weak optical confinement and hence single moded operation. Figure 1 is a schematic of a large cross section SOI rib waveguide as described by Soref. Low loss Waveguides of this type were soon demonstrated by several research groups [13].

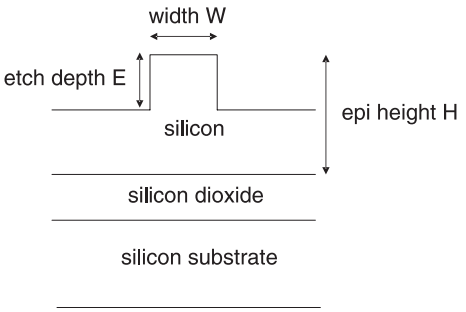

Fig. 1. The Silicon on Insulator rib waveguide geometry

Since these early demonstrations much research work has focussed upon waveguides fabricated in the SOI material system. Waveguides with dimensions varying from less than 1 μm [14] to several μm have been extensively researched. Complex active and passive devices have been demonstrated [15] and commercial products have been produced.

3 Waveguide Properties and Design

The design of optical waveguides in SOI materials requires the judicious selection of a number of structural parameters. The desired optical performance parameters, the manufacturing yield required and the cost and complexity of device packaging will all, to some extent, be influenced by these fundamental decisions. It is unlikely that there exists one best waveguide design for all applications. The intention here is not therefore to suggest practical waveguide designs but instead to consider the fundamental properties of SOI waveguides and to explain how these properties are influenced by the design decisions that are made.

The following paragraphs will first examine the modes of the silicon waveguide. The design criteria for single moded operation will be described. Design for compact waveguide bends and for the control of form birefringence will then be considered. Finally the impact of sidewall roughness upon SOI waveguides will be examined.

3.1 Modes of the SOI Waveguide

The correct operation of many waveguide device types is critically dependant upon the propagation of only a single guided optical mode. Higher order guided modes introduce cross-talk in Arrayed Waveguide Gratings (AWGs) [16], unexpected split ratios in Y-junctions and Multi-Mode-Interference devices (MMIs) and low extinction ratios in directional coupler type switches. In any complex waveguide based component light will inevitably, at

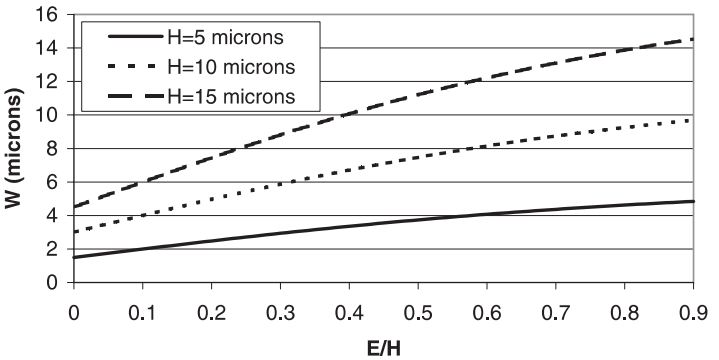

Fig. 2. The variation of single mode width with etch depth

some point, be scattered from the fundamental waveguide mode. This may occur at the optical fibre to waveguide interface, at a junction between straight and curved waveguides or in a straight waveguide itself due to scattering by lithographic roughness on the etched waveguide sidewalls. a primary design consideration is therefore that waveguides can be produced that will allow only a single guided mode to propagate with low loss.

Soref arrived at the following empirical single mode condition, valid when E/H is small, for the waveguide geometry of Fig. 1

$$\frac{W}{H} \leq 0.3 + \frac{H - E}{\sqrt{E^2 - 2HE}}\,. \tag{1}$$

Figure 2 plots the single mode condition for a variety of epitaxial layer thicknesses. The area below each line indicates the region of single mode operation according to the condition of (1).

From Fig. 2 it is clear that the thicker the epitaxial silicon layer that is employed the wider the range of rib widths that are available to the designer for single mode operation at the same slab to epitaxial layer ratio. Put another way as the epitaxial layer thickness increases so too does the etch depth required to achieve the same degree of optical confinement.

For most practical applications it is also important to be able to construct single mode waveguides which can achieve minimal bend radii with well controlled birefringence. Small bend radii allow for the fabrication of compact components and birefringence control is required for polarisation independent operation. The factors that influence these properties are now described.

3.2 Design of Curved Waveguides

The modal characteristics of curved SOI waveguides are, in general, quite different to those of straight waveguides of the same dimensions. The single mode condition described earlier is not appropriate for the design of curved

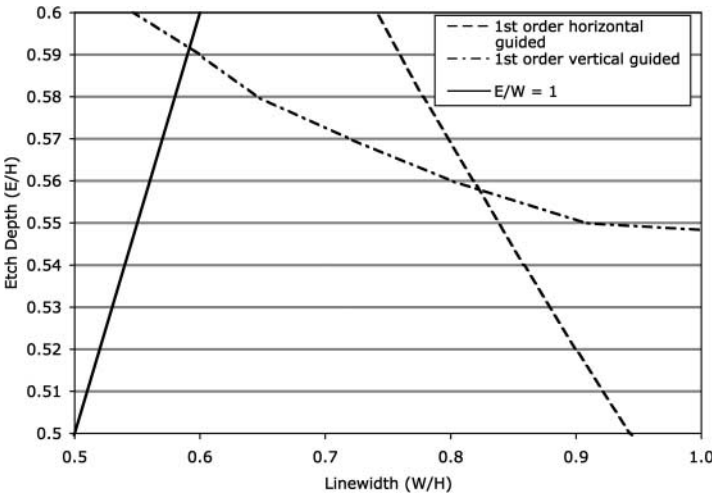

Fig. 3. The modal properties of an SOI waveguide with a 3 μm thick epitaxial layer

waveguides as the modal characteristics of these waveguides are heavily dependant upon the bend radius employed. Instead guided modes must be studied either by the use of a complex eigenmode solver or by the use of a propagation technique such as the Beam Propagation Method (BPM) [17].

Figure 3 summarises the results of TE polarised BPM simulations of a straight SOI waveguide with a 3 μm thick epitaxial layer. Figure 3 indicates the waveguide dimensions at which higher order modes begin to propagate with low loss. In addition, also shown on Fig. 3, is the condition at which the etch depth is equal to the rib width. There are manufacturing considerations that make it undesirable to fabricate guides where the etch depth exceeds the rib width. Figure 3 therefore indicates an available design region for single mode operation of a straight guide with a 3 μm thick silicon epitaxial layer.

Increasing the waveguide etch depth increases the confinement of the fundamental mode and reduces the radius of curvature that may be employed. From Fig. 3 the greatest practical etch depth for curved operation that allows for the design of single moded straight sections, in 3 μm thick epitaxial layers, can be obtained. Figure 4 below shows the radius of curvature at which the curved waveguide with this optimum etch depth begins to lose confinement of the fundamental TE mode as the waveguide width is varied. An excess bend loss of > 0.1 dB/cm is used to define this condition. Also shown in Fig. 4 are similar curves for waveguides with optimum etch depth calculated for other epitaxial layer thicknesses.

The decreasing bend propagation loss with guide width displayed by the waveguide geometry studied in Fig. 4 is characteristic of curved SOI waveguides. As the rib width is increased a whispering gallery mode results [18] at which point further increases in guide width do not further reduce guide loss.

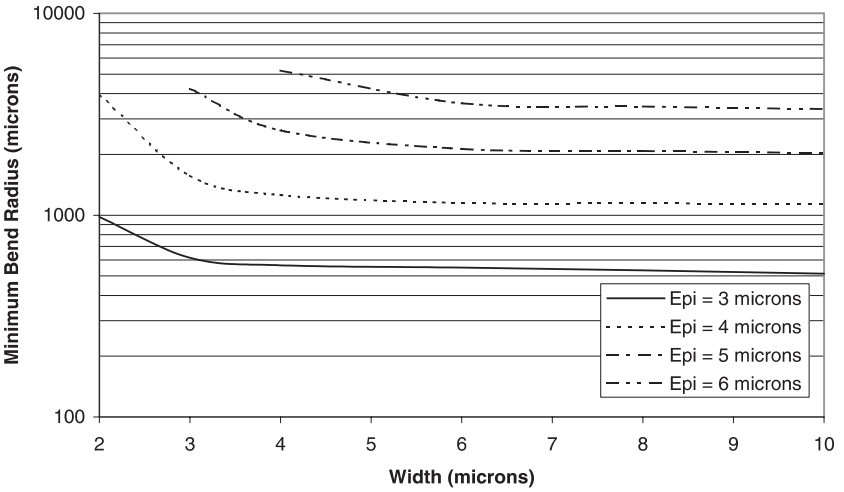

Fig. 4. Minimum practical radius of curvature waveguide bends as a function of width

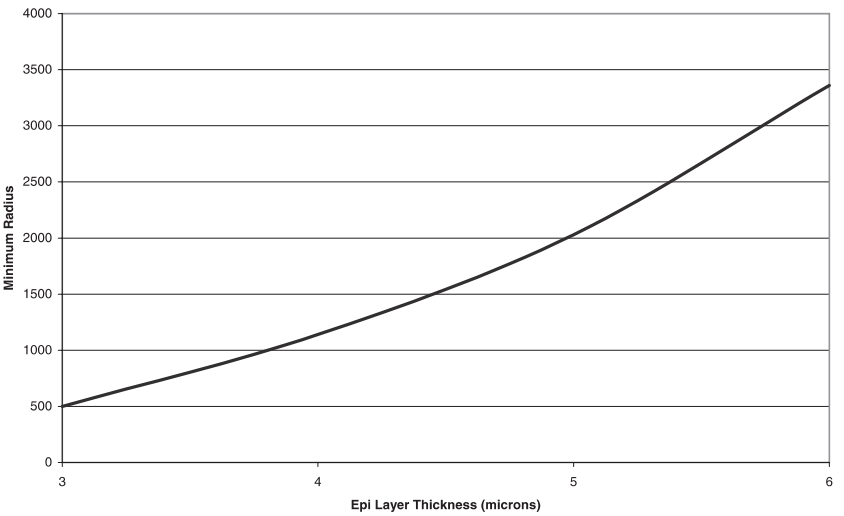

Fig. 5. The minimum achievable waveguide bend radius for a loss of less than 0.1 dB/cm as a function of epitaxial layer thickness

For a given epitaxial layer thickness and acceptable waveguide loss there is therefore a minimum limit upon the radius of curvature that may be achieved. Assuming an acceptable bend loss of 0.1 dB/cm of propagation Fig. 5 plots the radius of curvature below which this loss is exceeded as the epitaxial layer thickness is varied for the fundamental TE mode.

As the thickness of the selected silicon epitaxial layer is increased the practical minimum bend radius that can be achieved also increases.

3.3 Waveguide Birefringence Control

Most planar waveguide technologies produce waveguides with inherent birefringence. This birefringence may result from the properties of the waveguiding material itself [19], the fabrication processes used to construct the waveguide [20] or the asymmetry of the waveguide geometry [18]. As polarisation independent device operation is almost always essential it is most important to understand and control this fundamental waveguide property.

Most practically employed SOI waveguides are asymmetric leading to form birefringence. It can be shown, from electromagnetic theory [18], that form birefringence increases with the asymmetry of the waveguide geometry and also as the dimensions of the waveguide are reduced. In the following discussion the birefringence of the previously described waveguide geometry will be considered as the dimensions of the guide are varied.

Waveguide Birefringence is defined to be the difference between the modal indices of the fundamental Transverse Electric (TE) and Transverse Magnetic (TM) modes. In interferometric devices, such as arrayed waveguide gratings and Mach–Zehnder interferometers, birefringence manifests itself as a polarisation dependant shift (PDF) in the centre frequency of the device passband. Expressing birefringence as a frequency shift proves particularly useful when describing Dense Wavelength Division Multiplexed (DWDM) components. The birefringence induced frequency shift is here defined mathematically by the following equation where f_0 is the optical frequency.

$$\Delta f = 2\frac{N_{\mathrm{TM}} - N_{\mathrm{TE}}}{N_{\mathrm{TM}} + N_{\mathrm{TE}}} f_0 \,. \tag{2}$$

Consider now the birefringence of the single mode SOI waveguide described earlier. Figure 6 shows the birefringence of this waveguide, calculated using a polarised finite difference eigenmode solver, as the epitaxial layer thickness is varied.

As might be expected increasing the epitaxial layer thickness reduces the birefringence of the waveguide. In practise however it is more important to ensure that the birefringence is reproducible rather than minimal as techniques exist for on-chip birefringence compensation. In Fig. 7 the magnitude of the first derivative of the birefringence is plotted as the epitaxial layer thickness, waveguide width and etch depth are varied.

Waveguide designs with high derivatives in waveguide birefringence require tighter tolerances from fabrication processes in order to yield devices with acceptable birefringence. From the data presented in Fig. 7 it is straightforward to calculate the degree of fabrication process control required for a certain waveguide yield to a particular birefringence specification. For

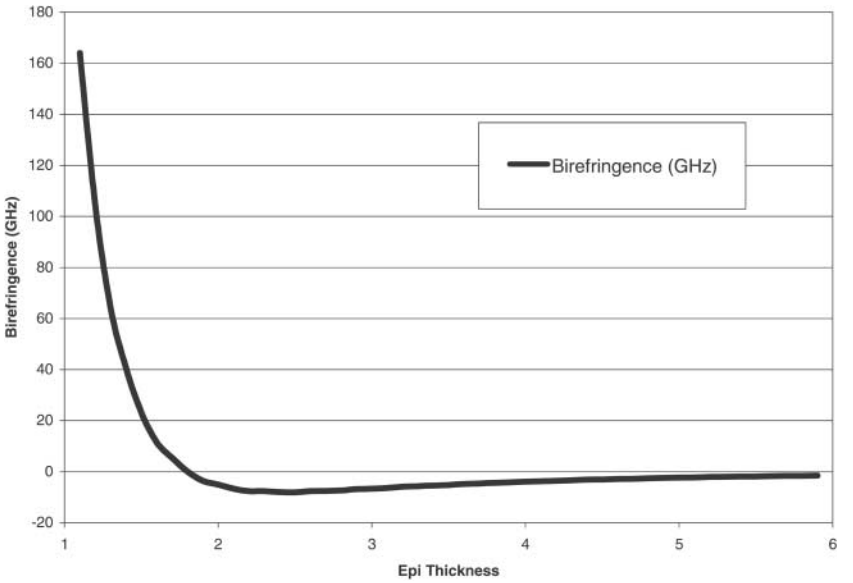

Fig. 6. Variation in waveguide birefringence with epitaxial layer thickness

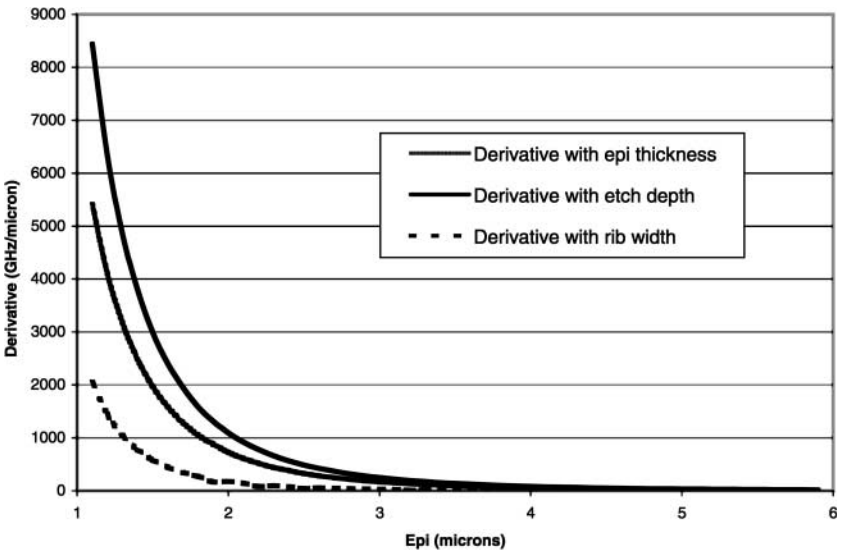

Fig. 7. Variations in the first derivative of the guide birefringence with waveguide dimensions

a possible specification consider the control of the passband centre frequency within a silicon arrayed waveguide grating. For a 100 GHz channel spacing system the useful grating passband widths are normally designed to

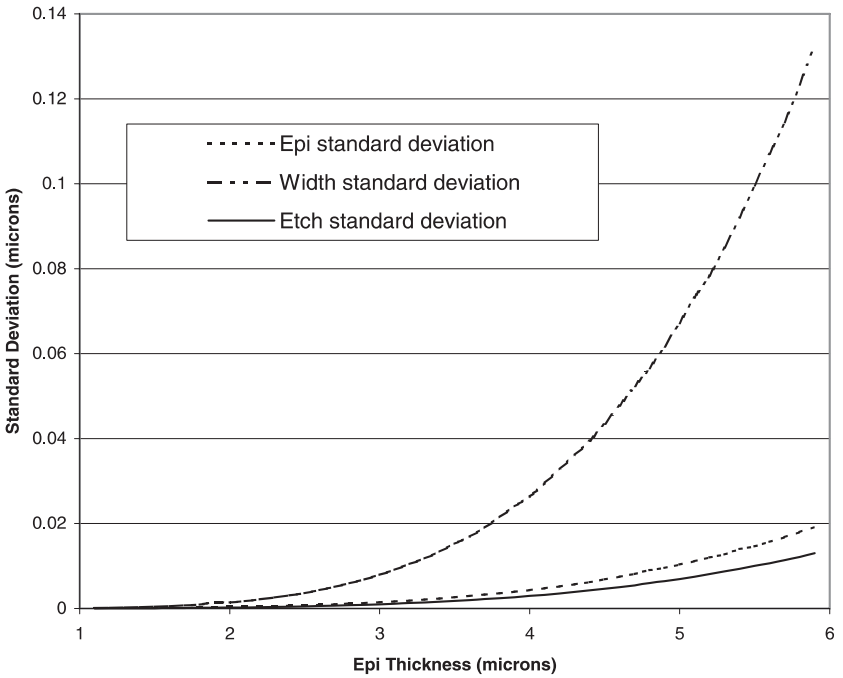

Fig. 8. Processing standard deviations required for a 0.25 GHz standard deviation in waveguide birefringence

be 25 GHz wide. The greater the variation in passband centre frequency with polarisation the smaller the usable bandwidth available within the system. System considerations suggest a reasonable standard deviation in passband centre frequency is around 1% of channel bandwidth, in this particular case 0.25 GHz. Figure 8 plots the process control required for a standard deviation in fabricated guide birefringence of 0.25 GHz.

The trend shown in Fig. 8 is generally true for single moded SOI waveguide geometries. The thinner the epitaxial silicon layer becomes the more difficult it becomes to control the birefringence of the fabricated waveguides.

3.4 Scattering Losses

Waveguide scattering losses result when propagating radiation interacts with roughly etched waveguide sidewalls. It is often assumed that scattering imposes severe limitations upon the loss performance that can be achieved in single mode high index contrast waveguides. This assumption originates from well known scattering theory which suggests that scattering losses should increase with the difference between the squared refractive indices of the waveguide core and cladding [21]. The magnitude of the scattering loss is however

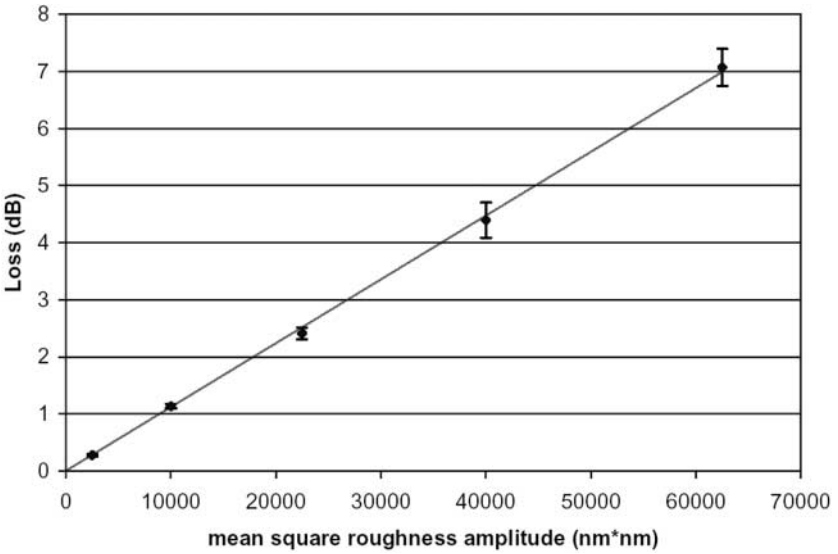

Fig. 9. Simulated scattering loss from an SOI rib waveguide as a function of the mean square roughness amplitude

also dependant upon the extent to which the guided mode interacts with the sidewall roughness.

SOI waveguides are normally designed with dimensions that are many times the wavelength of the guided radiation. The interaction of the guided mode with the etched sidewalls is therefore weak and, with typical levels of sidewall roughness, very low propagation losses are achieved. Roughness induced losses become problematic as the waveguide dimensions approach the wavelength, in silicon, of the guided radiation. Waveguides of these dimensions require special fabrication processes in order to reduce the amplitude of the roughness, and hence the loss, to acceptable levels [22].

It is possible to simulate the effects of sidewall roughness using the *Beam Propagation Method* [23]. Empirical studies have found that fabrication induced roughness displays an exponential autocorrelation function [24, 25]. Roughness of this form may be added to the sidewalls of a simulated rib waveguide and losses then calculated by averaging the losses of multiple beam propagation runs. Figure 9 shows the predicted waveguide propagation loss for an example SOI waveguide with a 4 μm epitaxial layer thickness, a 4 μm wide rib and a 2 μm deep etch as a function of the mean square sidewall roughness. a correlation length of 100 μm was assumed for the roughness used to generate Fig. 9.

The error bars on Fig. 9 indicate the range into which two thirds of the simulation results fall. As predicted by theory the propagation loss is found to be proportional to the mean square roughness amplitude. With modern

silicon microfabrication technology, rms roughnesses of less than 20 nm amplitude can typically be achieved without the use of non standard processing steps. For the simulated geometry, and most geometries used in practise, scattering losses of less 0.1 dB per cm are normally achieved.

3.5 Design Conclusions

The design of SOI waveguides requires a clear understanding of both the fabrication processes that will be used to construct the device and the ultimate performance that will be required. The selection of the appropriate waveguide geometry involves a compromise between the compactness of the complete device and the degree to which it is necessary to control the form birefringence. As a general rule the smaller the guide cross section the more difficult it becomes to control the form birefringence but the easier it becomes to fabricate compact components.

4 Interfacing Silicon Waveguides to Single Mode Fibres

Due to the high dielectric constant of silicon, single mode SOI waveguides may have optical field dimensions which are small in comparison to standard single mode optical fibre. As an example consider an SOI waveguide comprising a 4 μm thick silicon epitaxial layer, a 3 μm rib width and a 2 μm etch depth. Such a waveguide would have a fundamental mode with a mode field radius of 1.6 μm, compared to the fibre mode field radius of 5.2 μm. The coupling loss between this waveguide and the optical fibre would be in excess of 4.7 dB. To reduce the coupling loss of the fibre waveguide interface, it is necessary to use a mode transformer. The simplest mode transformer that can be used is to expand the waveguide horizontally. However, horizontal tapering only expands the field in one dimension and so the best coupling that can be achieved is with a 13 μm wide taper which gives a coupling loss of 3.1 dB.

To obtain a further improvement in coupling it is necessary to increase the height of the SOI waveguide. An SOI waveguide with a 12.5 μm thick silicon epitaxial layer, a 12.5 μm rib width and a 10 μm etch depth has a fundamental mode with a mode field radius of 4.8 μm and coupling loss to the fibre of 0.24 dB. Achieving such a low coupling loss enables SOI devices to be produced with losses comparable to other passive waveguide technologies such as silica on silicon, whilst still retaining all the advantages of the silicon material system. a single moded SOI waveguide which is sufficiently large to give good coupling efficiency to standard optical fibre will be unsuitable for the fabrication of compact waveguide bends and so will need to be tapered to smaller dimensions.

A schematic diagram of a taper that achieves low loss coupling is given in Fig. 10. The taper consists of two regions, there is a lower taper which is

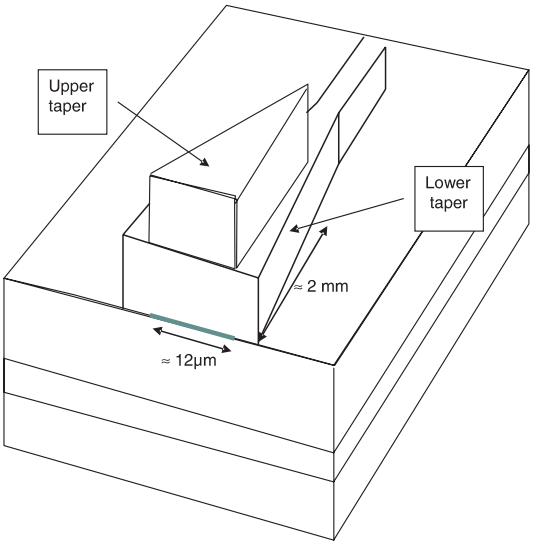

Fig. 10. Schematic of SOI taper to give low loss coupling to single mode fibre

about 20 µm wide, produced in 4 µm thick silicon etched to a depth of 2 µm. On top of this taper is an upper taper which is 12.5 µm high. Figure 11 shows how the light propagates along the taper. Initially the light is confined within the upper taper region, but at a width of around 6 µm, the light starts to transfer down and becomes a mode of the lower rib waveguide. This lower rib waveguide continues tapering beyond the end of the upper taper to produce the final single mode SOI waveguide with a 3 µm width. The total taper length is about 3 mm.

The taper is required to transform the fundamental mode of the optical fibre to that of the single mode SOI waveguide. When used in this way the taper is designed so that the fundamental waveguide mode propagates with minimal coupling to higher order modes if the waveguide is multimoded, or to radiation modes if it is single moded. A simple design approach for achieving this is to calculate the transmission of the fundamental mode through the taper as a function of the taper length L, using a beam propagation tool. The result will be a curve similar to that in Fig. 12.

From this curve the adiabatic limit is easily determined, and sets the taper length at which no significant mode coupling occurs. This approach is perfectly valid, and ensures low loss tapers. However, it will not produce a design of minimal length for a given loss. This is because a linear taper design, with constant taper angle, ignores the different rate of mode coupling along the taper, and consequently, at a given point along the taper, the taper angle may be larger than that needed to avoid unwanted mode coupling, making the taper longer than necessary. a rigorous approach to designing an optimal taper would be to solve the coupled mode equations along the taper.

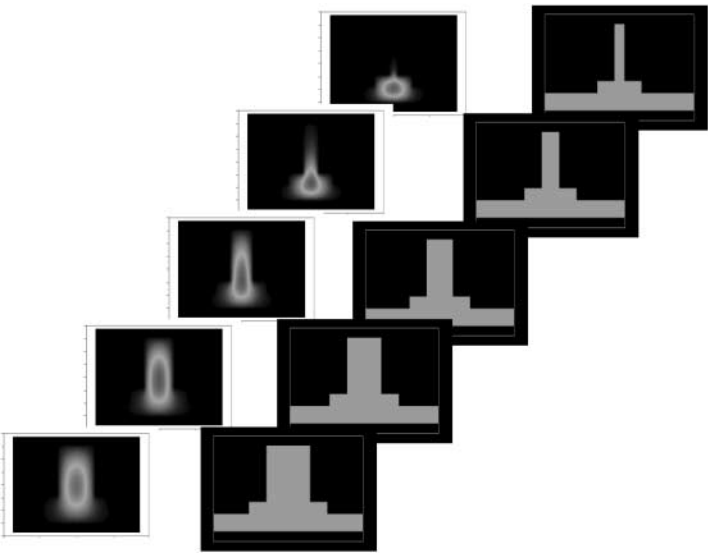

Fig. 11. Schematic of light propagation along taper

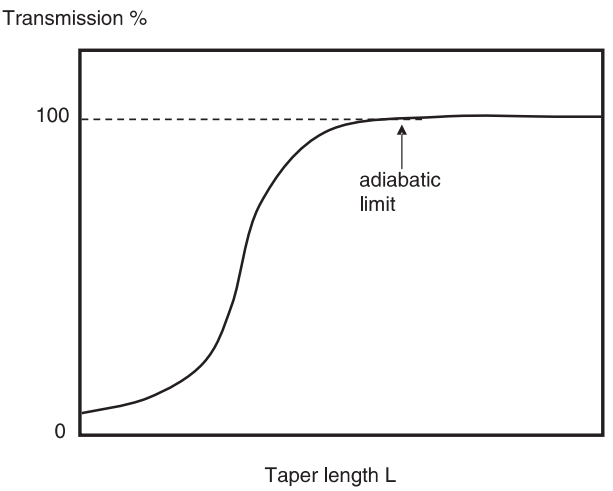

Fig. 12. Typical transmission through a taper as a function of taper length

However, this is unnecessarily complicated, and for most design purposes a simpler, more empirical approach can be used. This is based on the idea that for a taper to be adiabatic, the length scale over which its width varies should be long compared to the beat length between the fundamental mode and the nearest mode in effective index to which the fundamental can couple. Referring to Fig. 13, at a point z along the taper the waveguide half width

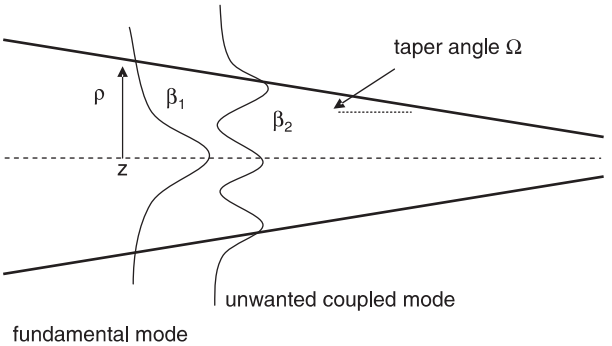

Fig. 13. Taper with coupling between fundamental mode and unwanted mode

is $\rho(z)$; the fundamental mode propagation constant is β_1, and the unwanted mode to which it can couple has propagation constant β_2.

The beat length between the modes is given by

$$L_{\mathrm{B}} = \frac{2\pi}{\beta_1 - \beta_2} \,. \tag{3}$$

The length scale over which the taper width is changing is

$$\rho \Big/ \frac{\mathrm{d}\rho}{\mathrm{d}z} \,. \tag{4}$$

The condition for an adiabatic taper is that (4) should be much greater than (3)

$$\rho \Big/ \frac{\mathrm{d}\rho}{\mathrm{d}z} \gg L_B \,. \tag{5}$$

Then from(3) we find that the local taper angle Ω must satisfy

$$\Omega = \frac{\mathrm{d}\rho}{\mathrm{d}z} \ll \frac{\rho}{L_{\mathrm{B}}} \,. \tag{6}$$

Equation (6), combined with (3), sets the adiabatic limit for a tapered waveguide. Because the beat length will vary with the waveguide half width ρ, we see from (6) that the limit on the taper angle will change with position along the taper, resulting in a taper with nonlinear profile. It should be emphasised that although the inequality in (6) is an empirical result, it can be shown that it sets an accurate limit on taper angle, and that tapers that exceed this limit will generally be lossy, and tapers which satisfy (6) will have low loss [26].

If the tapered waveguide supports only the fundamental mode, then loss will occur by coupling to radiation modes. In this case β_2 will be given by $n_2 k_0$

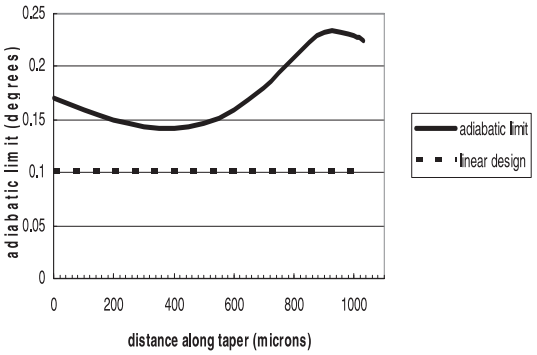

Fig. 14. Adiabatic limit

if the waveguide is surrounded by a medium of constant refractive index n_2; if it is a rib guide then the appropriate propagation constant will be that of the slab surrounding the rib.

An important point when applying (3) and (6) is understanding which modes couple. To answer this we consider the coupling coefficient C_{12} that defines mode coupling along the taper. It can be shown that C_{12} is given by [27]

$$C_{12} = \left(\frac{\varepsilon_0}{\mu_0}\right) \frac{k_0}{4} \frac{1}{\beta_1 - \beta_2} \int e_1 e_2 \frac{\partial n^2}{\partial z} \mathrm{d}A \,, \tag{7}$$

where e_1 and e_2 are the vector modal electric fields of the coupled modes, and n_2^2 is the refractive index distribution of the tapered waveguide at coordinate z along the taper. For most waveguides, n_2^2 only changes at the waveguide boundary. For example, for the tapered waveguide of Fig. 13 we see that $\partial n^2/\partial z$ is given by

$$\frac{\partial n^2}{\partial z} = \left(n_1^2 - n_2^2\right) \frac{\partial \rho}{\partial z} \delta\left(r - \rho(z)\right) \,, \tag{8}$$

where n_1 and n_2 are the core, cladding indices, and δ is the Dirac delta function. Consequently, the integral in (7) reduces to the sum of the products of the modal fields on each waveguide boundary which changes direction as a result of the taper. This means that only those modes that have the same symmetry with respect to the tapering waveguide boundaries can couple. It is important to remember that all the local modes along the taper retain their orthogonality, but can still couple because the integration in (7) reduces to the modal products on the waveguide boundary. Figure 14 shows an example of how the adiabatic limit varies along such a taper and shows that although the middle section requires an angle less 0.15°, the middle and end sections can use much larger angles, thereby resulting in a shorter taper for the equivalent loss.

Using the method described above, tapers have been fabricated which give a total pigtailed device loss less than 1 dB [28].

A second consideration at the fibre waveguide interface is back reflection from the waveguide into the fibre. There is large refractive index mismatch between the optical fibre (1.45) and the silicon (3.45), leading to both loss and back reflection. The Fresnel reflection at normal incidence is given by

$$R = \left(\frac{n_1 - n_2}{n_1 + n_2}\right)^2 . \tag{9}$$

Hence $R = -7.8\,\mathrm{dB}$ gives the back reflection and $1 - R = 0.79\,\mathrm{dB}$ gives the transmission loss. An anti reflection coating can be used to eliminate the transmission loss, but an angled interface is also required to reduce the back reflection to better than $-45\,\mathrm{dB}$. Introducing an angle between the fibre and waveguide leads to an additional complication due to refraction at the interface. The facet angle for the optical fibre θ_1 is given by

$$\theta_1 = \arcsin\left(\frac{n_2 sin(\theta_2)}{n_1}\right) . \tag{10}$$

For example if the silicon waveguide is fabricated to have a facet angle of 5°, the facet angle for the optical fibre is required to be 12°.

5 Silicon Arrayed Waveguide Gratings

5.1 Introduction

The arrayed waveguide grating concept was first reported by *Smit* [29] and *Dragone* [30], and demonstrated using SOI waveguide technology by *Jalali* [31]. The general design of such components in all planar technologies still follows that of Dragone, though numerous improvements have been published. In designing for the SOI platform we concentrate on achieving low loss and PDL, high crosstalk suppression, wide, flat passbands and a small footprint. Most importantly, these device properties must be tolerant to the manufacturing variations that result from an economical fabrication process.

5.2 Function

The well-known AWG layout consists of an input and an output star coupler that are interconnected by a number (or array) of waveguides. The Star couplers are constructed in such a way that an image of the field at the end of the input waveguide is reproduced somewhere along the output focal plane. However, the interconnecting waveguides are not all of the same length, but differ in length from the first through to the last by a fixed increment. This path length difference results in a wavelength dependence (or dispersion) of

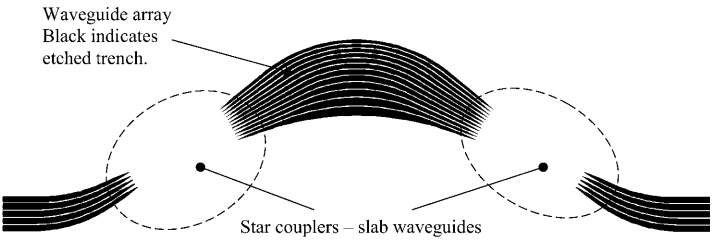

Fig. 15. AWG Schematic

the image position along the focal plane and allows the collection of different wavelength lights into different output waveguides. Hence the device functions as a wavelength demultiplexer or, if used in reverse, a multiplexer.

Rather than review the detailed design of SOI AWGs here, we will instead highlight the main ways in which they differ from those reported for the silica technology.

5.3 Loss Due to the Array-Slab Interface

The majority of the loss in the basic AWG device occurs at the two interfaces between the array waveguides and the slab waveguides. This is due to a mismatch between the array waveguide mode fields and the planar slab modes that travel parallel to them. In silica devices, the loss may be reduced by bringing the array waveguides close together where they join the slab waveguide and reducing their confinement [32]. This forces their optical modes to overlap each other, producing a resultant field that more closely matches a flat phase-front within the slab waveguide. This technique is less straightforward for SOI waveguides because the high refractive index contrast prevents the array waveguide modes overlapping within the etched regions. However, reduction of the ridge waveguide etch depth near to the interfaces allows the optical modes to overlap further and the loss to be substantially reduced [33,34,35]. By using a variation on the double-etch-depth scheme we are able to achieve losses of less than 0.5 dB and 1.0 dB for the centre and end channels respectively in a forty channel device.

5.4 PDF Control

A major advantage of the SOI waveguide technology is that birefringence is repeatable and can be controlled. In the absence of a waveguide cover material, modelling accurately predicts the measured value of the form birefringence. However, if a silicon dioxide cover layer is thermally-grown on the wafer, a strain is induced in the waveguide as the structure cools [36]. The birefringence is then modified and can even take the opposite sign to the form birefringence. Hence by patterning a film grown using a standard silicon oxidation process it is possible to create waveguides that have precise

birefringences of both signs and use them together to remove any polarisation-dependence in optical path lengths. In AWG devices PDF is maintained below 2 GHz by leaving the oxide cover over a part of each array waveguide and removing it elsewhere. However, the technique is only successful if the waveguide cross-sectional dimensions are relatively large (Sect. 3.3). This is because the form birefringence is greater and becomes far more sensitive to exact dimensions in smaller waveguides. Hence PDF variation due to process fluctuation is likely to become prohibitive if there is an attempt to manufacture devices constructed of low-dimensional waveguides.

5.5 Single Mode Design

It has been stated previously that relatively large waveguide cross-sections are required if the waveguide birefringence, and hence PDF, are to be controlled within acceptable limits. However, these dimensions result in slab waveguides that support the propagation of many guided modes with low loss. The presence of higher-order modes in a star coupler slab waveguide can lead to undesirable effects if the coupling to and from the ridge waveguides is not highly efficient. For instance, if the ridge-to-slab fundamental mode power coupling efficiency is 99% at each junction, then it might be assumed that the only consequence is a small loss. However, if the other 1% of power is not lost to radiation modes but transmitted across the coupler as the guided first-order slab mode, then it will interfere with the fundamental at the output. The slab waveguide birefringence will cause the result to differ between the TE and TM polarisations and there will be a Polarisation-Dependent Loss (PDL). In this example the PDL could be up to 0.175 dB, depending on the length and thickness of the slab waveguide and the wavelength of the light. Hence ridge-to-slab waveguide junctions must be designed very carefully in SOI technology if PDL is to be minimised. Fortunately it is possible to arrange for fundamental mode power coupling efficiencies in the region 99.7% by adiabatic tapering of the waveguide width before joining the slab waveguide. This guarantees that the PDL from this source is kept below approximately 0.05 dB.

5.6 Example Results

If the design measures described above are all taken, then SOI AWG devices can be manufactured that are entirely competitive with those in other technologies such as silica-on-silicon. Figure 16 shows the transmission spectrum of such an AWG. The device is designed to have clear passbands that are > 35 GHz wide and centred on 100 GHz-spaced ITU grid frequencies. This allows a large margin to guarantee that the product has 25 GHz-wide clear channels at the end-of-life under all ambient conditions. The on-chip loss at the edge of the worst band is less than 4.5 dB while the 1 dB bandwidths are

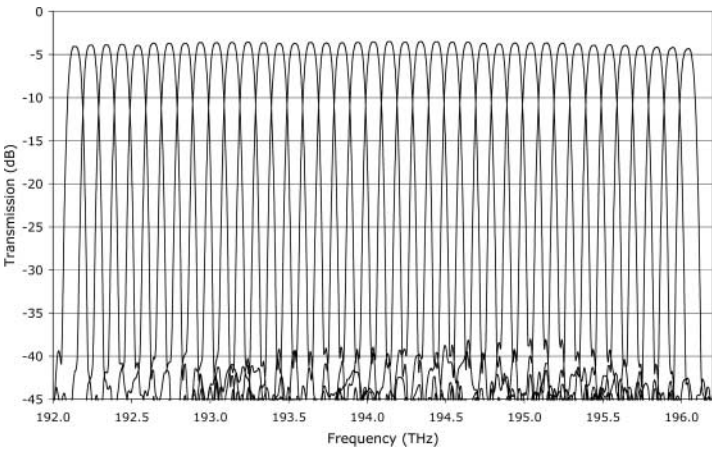

Fig. 16. Measured silicon AWG spectrum

all greater than 50GHz. The PDL across the bands is less than 0.3 dB, and the summed, worst-possible-case crosstalk < -24 dB (-29 dB typical).

6 The Silicon Variable Optical Attenuator

6.1 Mechanisms

Silicon has a cubic crystal structure, and therefore has no first order electrooptic effect. The second order electrooptic effect is small, as is the Franz–Keldish effect (change of band-gap with electric field). This leaves two practical options for bringing about a change in the propagation characteristics of light in silicon waveguides. Firstly, it is possible to exploit the dependence of refractive index on temperature, or thermooptic effect. Secondly, the refractive index and absorption coefficient of silicon may be changed by altering the concentration of electrons and holes, making use of the contribution made by free carriers to the optical constants of the semiconductor.

6.2 Thermooptic Effect

The thermooptic coefficient of silicon is $1.86 \times 10^{-4}\,^{\circ}\mathrm{C}^{-1}$. Thus a temperature rise of $5\,^{\circ}$C for example will increase the refractive index by $\Delta n \sim 10^{-3}$. The resulting phase shift per unit length of waveguide is $2\pi\delta n/\lambda$, where λ is the free-space wavelength, so that a heated waveguide length of the order of 1mm will provide a phase shift of π radians. By arranging that this phase shift takes place in one arm of an interferometer, an attenuator can be produced. a suitable configuration is the Mach–Zehnder interferometer, using Y-branches, evanescent couplers or multimode interference couplers to provide the functions of path splitting and combining.

In the example given above a temperature difference of approximately 5 °C must be maintained between two 1mm sections of waveguide in opposite arms of the interferometer, which will typically be separated by a distance of the order of 100 μm. The power required to maintain this temperature differential is approximately 300 mW, and the response time is in the range of tens of microseconds. a rough figure of merit, the product of power dissipation and response time, is approximately a hundred times lower than that for the corresponding silica waveguide system. As in silica technology it is possible to reduce the power requirement by improving the thermal isolation, for example by increasing the thickness of the buried oxide layer.

6.3 Free Carrier Effects

In general the optical properties of a semiconductor in the visible and infrared regions of the spectrum are dominated by absorption due to bound electrons at photon energies below the band-gap, which for silicon corresponds to a wavelength of 1.1 μm. At wavelengths shorter than 1.1 μm the optical absorption coefficient is therefore very high, while at higher wavelengths there is no longer any contribution from bound electrons. There is still, however, a contribution from free carriers, which may be visualised as follows.

In the simplest, classical approximation, free carriers in the semiconductor can be considered to respond to the accelerating force provided by an electric field, and also to the viscous damping, or momentum relaxation, experienced as the aggregate result of the various carrier scattering mechanisms. This is the well-known Drude approximation, which leads to the following expression for conductivity:

$$\sigma = \frac{Ne^2\tau/m^*}{1+\omega^2\tau^2}(1+i\omega)\,, \tag{11}$$

where the symbols have the following meaning:

σ	electrical conductivity	N	carrier concentration
e	electronic charge	τ	momentum relaxation time
m^*	carrier effective mass	ω	angular frequency

In this convention the real part of the conductivity is derived from the component of carrier velocity which is in phase with the applied electric field, and which leads to familiar expressions for dc conductivity and carrier mobility. It is this component of velocity which is responsible for the absorption of energy from the field, giving rise to electrical resistance at low frequencies and to attenuation at optical frequencies.

At frequencies comparable to the momentum relaxation rate, $1/\tau$, the carrier velocity begins to lag behind the driving field, and a quadrature component of velocity develops, which is represented by the imaginary part of the conductivity.

If the displacement of carriers is considered instead of their velocity, then corresponding expression is obtained for the polarisation generated by the free carriers, and hence the dielectric constant:

$$\varepsilon_r = 1 - \frac{Ne^2\tau^2/\varepsilon_0 m^*}{1+\omega^2\tau^2}\left(1+\frac{i}{\omega\tau}\right). \tag{12}$$

Since the carrier velocity and displacement are in quadrature, the real component of the conductivity, which is associated with attenuation, corresponds to the imaginary component of dielectric constant, and vice-versa. As the frequency increases and the carrier velocity begins to lag behind the driving field, the component of displacement which develops is in antiphase with the field. In other words the effect of carrier motion is to reduce the real part of the dielectric constant.

The momentum relaxation time, τ lies in the picosecond range, so that in the infrared and optical regions of the spectrum the condition $\omega\tau \gg 1$ holds, from which the following approximations for refractive index and absorption can be deduced:

$$\delta_n = -\frac{e^2\lambda^2 N}{8\pi^2 c^2 \varepsilon_0 n m^*} \tag{13}$$

$$\delta_\alpha = -\frac{e^3\lambda^2 N}{4\pi^2 c^3 \varepsilon_0 n \mu m^{*2}} \tag{14}$$

where

δ_α change in absorption coefficient due to free carriers
δ_n change in refractive index due to free carriers
n background refractive index
λ free space wavelength.

The total free carrier contributions to refractive index and absorption are given by adding the terms for electron and hole contributions.

In order to improve upon this simple description of free carrier effects it is necessary to apply a quantum mechanical treatment, and to consider the various scattering mechanisms individually. An accurate empirical formula has been reported [37], in which the changes in refractive index and absorption coefficient due to free carriers are given as follows

$$\Delta n = -\left(8.8\times10^{-22}N_e + 8.5\times10^{-18}\times N_h^{0.8}\right) \tag{15}$$

$$\Delta \alpha = 8.5\times10^{-18}N_e + 6.0\times10^{-18}\times N_h\,. \tag{16}$$

These relations are plotted in Fig. 17.

6.4 Pin Diode Attenuator

It is clear from figure that a necessary condition for waveguide transparency is that the carrier concentration in the passive waveguide should be low. For

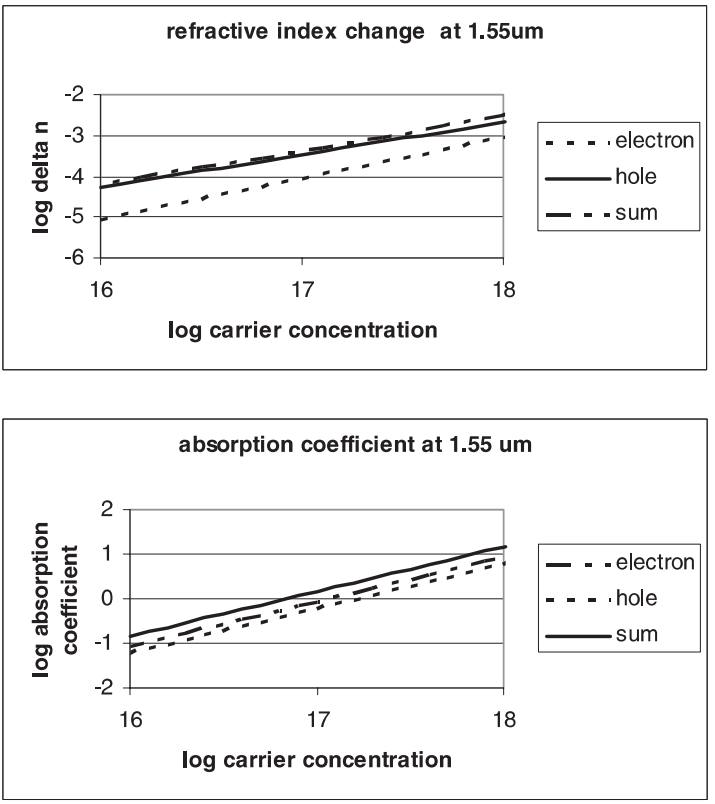

Fig. 17. The dependence of refractive index and absorption length on free carrier concentration

example to achieve absorption below $0.1\,\mathrm{dB}\cdot\mathrm{cm}^{-1}$ (an absorption coefficient of less than $0.02\,\mathrm{cm}^{-1}$) a doping level below 10^{-15} is required. Starting from a passive silicon waveguide a sufficiently low carrier concentration, a convenient way in which to vary the carrier concentration within the waveguide is to fabricate a pin diode with the cross-section shown in Fig. 18. This structure allows the carrier concentration to remain low in the inactive state, but to increase on application of a forward bias, whereupon electrons are injected from the n region and holes from the p region. Care must be taken to locate the doped regions sufficiently far from waveguide (in practice several μm) in order to prevent passive loss which would result from exposure of the optical mode to the doped regions.

The pin diode device can be used to control refractive index, and hence produce attenuation via an interferometer, as in the example of a thermooptic interferometric attenuator described above. Alternatively, the absorption due to free carriers can be used directly to produce attenuation in a section of plain waveguide. From the relations of figure it can be deduced that

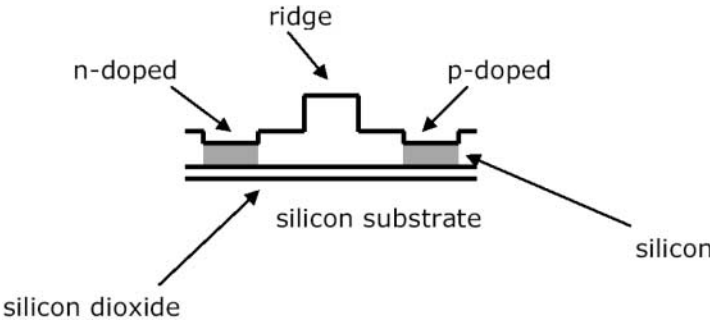

Fig. 18. Cross-section through a waveguide pin diode attenuator

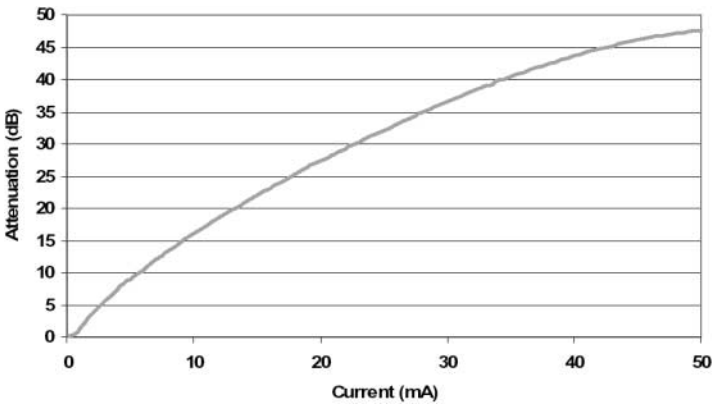

Fig. 19. Attenuation vs current characteristic of four 2.5 mm section pin diode attenuator

a carrier concentration of $10^{18}\,\mathrm{cm}^{-3}$ will produce attenuation of $50\,\mathrm{dB}\cdot\mathrm{cm}^{-1}$ (an absorption coefficient of $10\,\mathrm{cm}^{-1}$) so that a high level of attenuation can be produced in a convenient length of waveguide. The current required to achieve this concentration is of the order of $200\,\mathrm{mA}\cdot\mathrm{cm}^{-1}$ of waveguide length. In practice it is usual to divide the length of the waveguide pin diode into a number of sections and feed the individual diodes in series, thus allowing a convenient voltage/current operating range to be achieved. Figure 19 shows the attenuation vs current characteristics of such a device in which a 10-mm long device is divided into four sections fed in series. Consequently the operating voltage is in the range 3 V to 4 V. Power dissipated at 50 dB attenuation is approximately 200 mW.

An advantage of the absorption attenuator is the high level of extinction possible, and the low polarisation dependence which can be achieved over the entire attenuation range. Both of these parameters are more difficult to control in Mach–Zehnder interferometer based devices, where the photonic properties of the interferometer limit performance.

One of the design aims of the pin diode attenuator is to minimise the current required to provide a given carrier density within the waveguide. This is achieved in practice in the design of figure by etching trenches before introduction of the dopant by ion implantation, in order that the doped regions extend throughout the depth of the SOI layer. This precaution ensures eliminates the 'wasted' current which would otherwise flow if carriers of both polarities were able to escape from the device and diffuse sideways away from the waveguide.

The response time of the pin diode attenuator is governed by the transit time of carriers across the waveguide, and for the device illustrated it is typically in the submicrosecond range. Modulation at frequencies in excess of 100 MHz has been predicted for waveguide pin diodes of cross-sectional dimensions of the order of a few micrometer [38].

References

1. S. V. Kartalopoulos: *Introduction to DWDM Technology* (IEEE Press 2000)
2. D. J. Blumenthal: Integrated devices for wavelength-agile all-optical networks, Integrated photonics research technical digest (2002)
3. K. Maru, T. Chiba, T. Hasegawa, K. Tanaka, H. Nonen, H. Uetsuka: High resolution dynamic gain equalizer using super-high Δ planar lightwave circuit technology, Optical Fiber Communication Conference (OFC) Proceedings (2003), 172–173
4. H. Nishihara, M. Haruna, T. Suhara: *Optical Integrated Circuits* (McGraw-Hill 1997)
5. M. Kawachi: Silica waveguides on silicon and their application to integrated-optic components, Optical and Quantum Electronics **22**, 391–416 (1990)
6. R. Soref: Silicon-Based Optoelectronics, Proceedings of the IEEE **81**, 1687–1706 (1993)
7. S. Suzuki, M. Yanagisawa, Y. Hibino, K. Oda: High-density integrated planar lightwave circuits using SiO_2-GeO_2 waveguides with a high refractive index difference, Journal of Lightwave Technology **12**, 790–796 (1995)
8. R. Soref, J. P. Lorenzo: All-silicon active and passive guided-wave components for $\lambda = 1.3$ E and 1.6 μm, IEEE Journal of Quantum Electronics **22** (1986)
9. J. P. Colinge: *Silicon-On-Insulator Technology: Materials to VLSI* (Kluwer Academic Publishers 1997)
10. S.S. Iyer, A.J. Auberton-Herve (Eds): *Silicon Wafer Bonding Technology for VLSI and MEMs* (EMIS Processing Books 2001)
11. T. M. Benson, M. Burnham, D. E. Davis, N. Mohd Kassim, M. Seifouri: Single-Mode Optical Waveguides in Silicon, IEEE Colloquium Digest 1989/93, Integrated Optics, 11/1–11/4 (1989)
12. R. Soref, J. Schmidtchen, K. Petermann: Large Single-Mode Rib Waveguides in GeSi-Si and Si-on-SiO_2, IEEE Journal of Quantum Electronics **8**, 1971–1974 (1991)
13. A. Rickman, G. Reed, F. Namavar: Silicon-on-insulator optical rib waveguide loss and mode characteristics, Journal of Lightwave Technology **12**, 1771–1776 (1994)

14. K. K. Lee, D. R. Lim, L. C. Kimerling: Fabrication of ultralow-loss Si/SiO_2 waveguides by roughness reduction, Optics Letters **26**, 1888–1890 (2001)
15. I. E. Day, S. W. Roberts, R. O'Carroll, A. Knights, P. Sharp, G. F. Hopper, B. J. Luff, M. Asghari: Single-chip variable optical attenuator and multiplexer subsystem integration, in Optical Fiber Communication Conference (OFC) Proceedings (2002), 72–73
16. M. K. Smit, C. V. Dam: PHASAR-Based WDM-Devices: Principles, Design and Applications, IEEE Journal of Selected Topics in Quantum Electronics **2**, 236–250 (1996)
17. R. Scarmozzino, A. Gopinath,R. Pregla, S. Helfert: Numerical Techniques for Modeling Guided-Wave Photonic Devices, IEEE Journal of Selected Topics in Quantum Electronics **6**, 150–162 (2000)
18. C. Vassallo: *Optical Waveguide Concepts* (Elsevier 1991)
19. R. G. Hunsperger: *Integrated optics: theory and technology* (Springer 1984)
20. M. Kawachi: Silica waveguides on silicon and their application to integrated-optic components, Optical and Quantum Electronics **22**, 391–416 (1990)
21. R. C. Hewson-Browne, P. C. Kendall, D. A. Quinney: Roughness scattering into substrate radiation modes of rib waveguides, IEE Proceedings J. **136**, 281–286 (1986)
22. K. K. Lee, D. R. Lim, L. C. Kimerling: Fabrication of ultralow-loss Si/SiO_2 waveguides by roughness reduction, Optics Letters **26**, 1888–1890 (2001)
23. G. H. Jin, J. Harari, L. Joannes, J. P. Vilcot, D. Decoster: Numerical analysis of the radiation losses due to surface roughness in integrated optics devices, IEEE Photonics Technology Letters **8**, 1202–1204 (1996)
24. F. Ladouceur, J. Love, T. Senden: Effect of side wall roughness in buried channel waveguides, IEE Proceedings J. **141**, 242–248 (1994)
25. F. Payne: private communication (2002)
26. J. Love: Application of a low loss criterion to optical waveguides and devices, IEE Proceedings J **136**, 225–228 (1989)
27. A. W. Snyder, J. D. Love: *Optical Waveguide Theory* (Chapman and Hall, 1993)
28. I. Day, I. Evans, A. Knights, F. Hopper, S. Roberts, J. Johnston, S. Day, J. Luff, H. Tsang, M. Asghari: Tapered silicon waveguides for low insertion loss highly efficient high speed electronic variable optical attenuators, Optical Fiber Communication Conference (OFC) Proceedings (2203), pp. 249–250
29. M. K. Smit: New focussing and dispersive planar component based on an optical phased array, Electronics Letters **34**, 385–386 (1988)
30. C. Dragone: An $N \times N$ optical multiplexer using a planar arrangement of two star couplers, IEEE Photonics Technology Letters **9**, 812–815 (1991)
31. P. D. Trinh, S. Yegnanarayanan, F. Coppinger, B. Jalali: Silicon-on-insulator (SOI) phased-array wavelength multi-demultiplexer with extremely low-polarisation sensitivity, IEEE Photonics Technology Letters **9**, 940–942 (1997)
32. J. C. Chen, C. Dragone: A study of fibre-to-fibre losses in waveguide grating routers, Journal of lightwave technology **15** (1997)
33. C. van Dam: Loss reduction for phased-array demultiplexers using a double etch technique, Integrated Photonics Research Proceedings, 52–55 (1996)
34. C. G. Herben: Low-loss and compact phased array demultiplexers using a double etch process, Proceedings of the 9th Conference on integrated optics (ECIO 1999), pp. 211–214

35. J. H. den Besten: Low-loss, Compact, and polarisation independent PHASAR demultiplexer fabricated by using a double-etch process, IEEE Photonics Technology Letters **14**, 62–64 (2002)
36. Bookham Technology plc patent entitled *Waveguide birefringence control using thermal oxide*
37. R. Soref, B. R. Bennett: IEEE Journal of Quantum Electronics **23** (1987)
38. A. Vonsovici, A. Koster: IEE Journal of Lightwave Technology **17** (1999)

Index